Probing PAH formation chemical kinetics from benzene and toluene pyrolysis in a single-pulse shock tube

Wenyu Sun, Alaa Hamadi, Said Abid, Nabiha Chaumeix, Andrea Comandini

Available online at www.sciencedirect.com
ScienceDirect
Proceedings of the Combustion Institute 000 (2020) 1–10
Proceedings of the Combustion Institute
www.elsevier.com/locate/proci

Probing PAH formation chemical kinetics from benzene and toluene pyrolysis in a single-pulse shock tube ☆

Wenyu Sun [a,*], Alaa Hamadi [a], Said Abid [a,b], Nabiha Chaumeix [a], Andrea Comandini [a,*]

[a] *CNRS-INSIS, I.C.A.R.E., 1C, Avenue de la recherche scientifique, 45071 Orléans cedex 2, France*
[b] *Université d'Orléans, 6 Avenue du Parc Floral, 45100 Orléans, France*

Received 6 November 2019; accepted 28 June 2020
Available online xxx

Abstract

Benzene and toluene were pyrolyzed under highly argon-diluted conditions at a nominal pressure of 20 bar in a single-pulse shock tube coupled to gas chromatography/gas chromatography–mass spectrometry (GC/GC–MS) diagnostics. Concentration evolutions of polycyclic aromatic hydrocarbon (PAH) intermediates were measured in a temperature range of 1100–1800 K by analyzing the post-shock gas mixtures. Different PAH speciation behaviors, regarding types, concentrations and formation temperature windows, were observed in the two reaction systems. A kinetic model was proposed to predict and interpret the measurements. Through a combination of experimental and modeling efforts, PAH formation patterns from species pools of benzene and toluene pyrolysis were illustrated. In both cases, channels leading to PAHs basically originate from the respective fuel radicals, phenyl and benzyl. Due to the higher thermal stability of benzene, the production of phenyl, and thus most PAH species, occur in higher temperature windows, in comparison to the case of toluene. In benzene pyrolysis, benzyne participates in the formation of crucial PAH species such as naphthalene and acenaphthylene. Phenyl self-recombination takes considerable carbon flux into biphenyl, which serves as an important intermediate leading to acenaphthylene through hydrogen loss and ring closure. The resonantly-stabilized benzyl is abundant in toluene pyrolysis, and its decomposition further produces other resonantly-stabilized radicals such as fulvenallenyl and propargyl. Barrierless addition reactions among these radicals are found to be important sources of PAHs. Fuel-specific pathways have pronounced effects on PAH speciation behaviors, particularly at lower temperatures where fuel depletion is not completed within the reaction time of 4.0 ms. Contributions from the commonly existing Hydrogen-Abstraction-Carbon-Addition (HACA) routes increase with the temperature in both cases.

Keywords: Single-pulse shock tube; Benzene; Toluene; Pyrolysis; Polycyclic aromatic hydrocarbons (PAHs)

☆ Colloquium: GAS-PHASE REACTION.

* Corresponding authors.
E-mail addresses: wenyu.sun@cnrs-orleans.fr (W. Sun), andrea.comandini@cnrs-orleans.fr (A. Comandini).

https://doi.org/10.1016/j.proci.2020.06.077

1. Introduction

Predictive kinetic models describing polycyclic aromatic hydrocarbons (PAHs) formation in gas phase are required for the development of clean combustion technologies. Challenges remain in clarifying the complicated reaction network in combustion systems. The finding through recent studies [1,2] that the fuel pyrolysis and the oxidation of resulting products are separated processes can potentially decouple the kinetic complexity. Benzene (C_6H_6) and toluene (C_7H_8), the simplest aromatic compounds, are essential components of practical or surrogate fuels as well as important combustion intermediates. Thus, it is fundamental and obligatory to thoroughly understand the PAH formation chemistry in benzene and toluene pyrolysis.

Previous studies focused on the pyrolysis chemical kinetics of both fuels. Speciation information, mostly for small molecules relevant to fuel decompositions, was obtained from shock tube experiments [3–5], and aided by high-level theoretical investigations [6–8], the fuel decomposition patterns of benzene and toluene were gradually well-established. On this basis, continuous efforts were made to explore the related PAH formation chemistry. Shock tube pyrolysis experiments [9,10] were conducted using phenyl iodide as a precursor of phenyl (C_6H_5), the fuel radical of benzene. Meanwhile, relevant PAH formation pathways were proposed and corresponding kinetic parameters were refined through theoretical calculations [10–12]. Uncertainties nevertheless remain and it is useful to further investigate PAH formation pathways via direct benzene pyrolysis experiments. Regarding toluene, Shulka et al. [13] performed low-pressure pyrolysis experiments in a flow reactor, and PAHs with mass numbers up to 522 were detected with a mass spectrometer. Matsugi and Miyoshi later proposed a kinetic model [14] based on their theoretical calculations [15,16] to interpret the measurements for two to three ring aromatics reported in [13]. Yuan et al. [17] also conducted toluene pyrolysis experiments in a flow tube reactor and discussed the formation pathways of measured PAHs with a detailed kinetic model. However, the above-mentioned flow reactor pyrolysis experiments were carried out at atmospheric or subatmospheric pressures. The roles of the proposed pathways under high pressure conditions more relevant to practical combustion still need to be revealed.

The goal of this work is to provide reliable speciation datasets using shock tube and gas chromatographic (GC) techniques and to develop a predictive kinetic model for benzene and toluene pyrolysis, with emphasis on detailed formation mechanisms of two- to four-ring PAH intermediates. With the combination of experimental measurements and modeling analysis, kinetic insights regarding common as well as fuel-specific PAH formation pathways will be presented.

2. Shock tube pyrolysis experiments

2.1. Experimental setup

The experimental facility used in this work was constructed based on the set-up developed by Comandini et al. [18]. The apparatus is composed of a single-pulse shock tube with a driven section 78 mm in inner diameter and 6.0 m in length, and a gas chromatography/gas chromatography–mass spectrometry (GC/GC–MS) system, as the schematic provided in **Fig. S1** in the ***Supplemental Material***. The driven section of the shock tube was heated up to 90 °C to avoid the condensation of fuels and heavy products. To operate the shock tube in single-pulsed fashion, a dump tank with the volume of 150 L was placed close to the double diaphragm section on the driven section side. Four pressure sensors (CHIMIE METAL A25L05B) were mounted along the last part of the driven section and spaced at 150 mm with the last one being 82 mm away from the endwall. The time taken for the shock wave to pass each interval was used to derive the velocity of the incident wave, for the subsequent calculation of the pressure and temperature conditions behind the reflected shock wave (P_5 and T_5), by solving the conservation equations. The uncertainty in the calculated T_5 was within ±30 K, based on the error in the distances between pressure sensors which have a diameter of 2 mm. The post-shock gas mixtures were sampled with an air-actuated HIP valve, which takes hundreds of milliseconds to open and close. Fast sampling would not be possible as large sample pressures were required for sufficient sensitivity of the trace PAH species (10^{-2} ppm). Since the volume of the withdrawn gas was relatively large, the average velocity was used to calculate T_5 and P_5, which are more representative of the conditions encountered by the sampled gas, compared to those calculated with the extrapolated velocity at the endwall. Besides, the attenuation in the velocity was below 2.5% for most experiments, so the difference between the averaged or the extrapolated T_5 was below 20 K, within the uncertainty specified above. A PCB pressure sensor shielded by a layer of RTV was located on the endwall to record the pressure time history, from which the reaction time could be defined, as detailed in [19]. A typical pressure profile is shown in Fig. 1 and the reaction time with the current experimental configuration is around 4.0 ms.

The sampled mixtures were transferred through a SilcoTek line heated at 150 °C for subsequent composition analyses. The analytical system consisted of two GCs placed in series. The first one (Agilent 7890) was equipped with a flame ioniza-

Please cite this article as: W. Sun, A. Hamadi and S. Abid et al., Probing PAH formation chemical kinetics from benzene and toluene pyrolysis in a single-pulse shock tube, Proceedings of the Combustion Institute, https://doi.org/10.1016/j.proci.2020.06.077

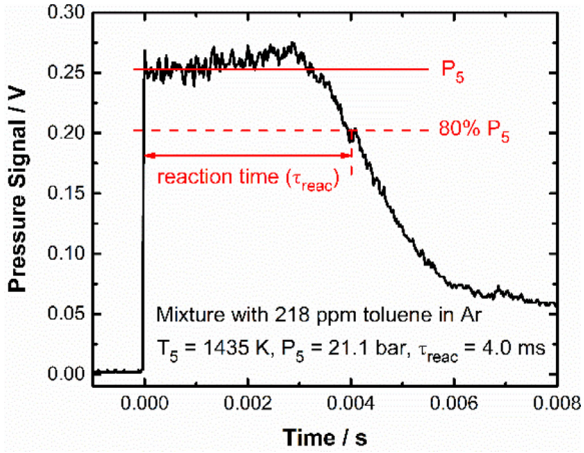

Fig. 1. Typical endwall pressure history at nominal 20 bar and the definition of reaction time.

tion detector (FID) coupled to a DB-17-ms column for heavy species separation, and a thermal conductivity detector (TCD) coupled to a Molsieve 5A column to monitor the absence of air. To effectively recover and measure the heavy compounds, the GC valves and the corresponding sample loops, where gas samples are stored before injection into the column, were placed in an external oven which could regulate the temperature to 250 °C. The second GC (Thermo Trace GC Ultra) was equipped with an FID connected to an HP Plot Q column to measure light species and a TCD to detect the internal standard neon. A DSQ mass spectrometer was also connected to the second GC to aid the species identification when needed. Most detected PAH species were identified thanks to the combination of the retention time of known samples and the fragmentation patterns in the mass spectra. Standard gas mixtures were used for the calibration of light species including C_2–C_5 hydrocarbons except diacetylene (C_4H_2), for which the calibration factor was obtained from acetylene (C_2H_2) decomposition experiments through carbon atom conservation. For fuels and relatively small aromatics [including phenylacetylene ($C_6H_5C_2H$), styrene ($C_6H_5C_2H_3$), indene (C_9H_8), naphthalene ($C_{10}H_8$), biphenyl ($C_6H_5C_6H_5$), bibenzyl ($C_6H_5C_2H_4C_6H_5$) and acenaphthalene ($AC_{12}H_8$)], calibrations were performed with gas-phase mixtures prepared in a heated (150 °C) glass vessel to minimize the surface absorption. While for larger PAH species, the gas-phase calibration factors were deduced from their signal intensities relative to that of naphthalene through liquid-phase calibration. The calibration and the FID response were the major uncertainty sources of concentration measurements. For species calibrated in gas phase, an uncertainty of less than 10% was expected, and for larger species without direct gas-phase calibrations, the uncertainty factor varies from 20% to a factor of 2, depending on the species molecular weights relative to naphthalene [18].

Experiments were performed at the nominal P_5 of 20 bar with two argon-diluted mixtures respectively containing 200 ppm of benzene and toluene, which were prepared in a 136 L electropolished stainless steel cylinder with neon added as an internal standard. The inner surface of the driven section is cleaned every day to remove potential soot deposits. Experimental results in this work, including the calculated T_5 and P_5, reaction time, species concentrations as well as the measured pressure profile for each shock tube operation, are provided in the ***Supplemental Material***. Test experiments for *n*-heptane pyrolysis at the initial fuel concentration of 100 ppm were carried out at the nominal P_5 of 10 bar with T_5 ranging from 900 to 1800 K. The species concentration profiles were compared with predictions by different extensively-validated kinetic models, as shown in **Fig. S2** in the ***Supplemental Material***. The good agreement between the measurements and simulations on both shapes and sizes of the profiles confirms the reliability of the current set-up.

2.2. PAH species detection

In this work, PAH species up to C_{18} were detected and the signal peaks were well separated till chrysene and its isomers. Larger PAH species, which were beyond the detection capability of our system, might condense. Soot formation is probable since the experiments were performed under high-pressure, pyrolytic conditions with aromatic fuels, but the amounts of produced particles should be limited by the low fuel concentrations. GC signals for heavy compounds produced from benzene and toluene pyrolysis under selected conditions are displayed in Fig. 2. The pyrolysis of toluene and benzene share

Please cite this article as: W. Sun, A. Hamadi and S. Abid et al., Probing PAH formation chemical kinetics from benzene and toluene pyrolysis in a single-pulse shock tube, Proceedings of the Combustion Institute, https://doi.org/10.1016/j.proci.2020.06.077

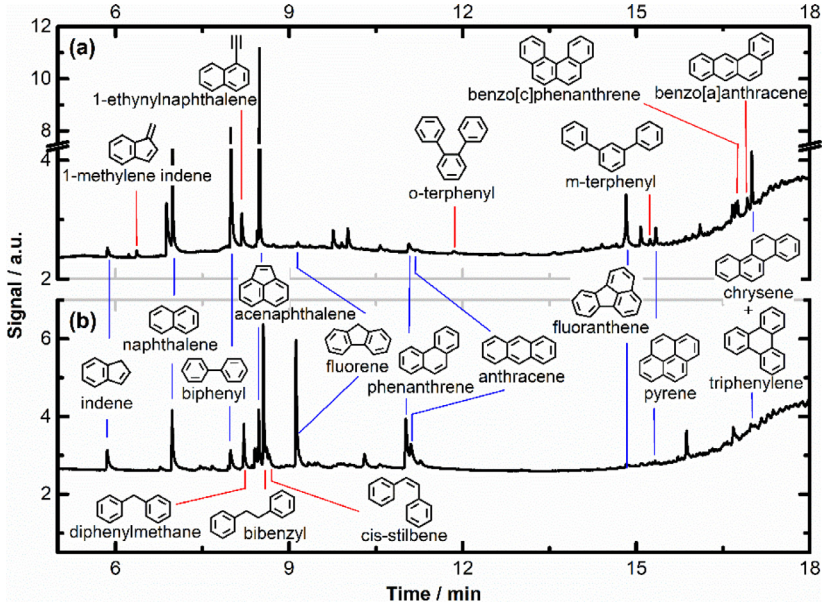

Fig. 2. GC signals for PAH species detected in (a) benzene pyrolysis at $T_5 = 1553$ K, $P_5 = 21.8$ bar and (b) toluene pyrolysis at $T_5 = 1435$ K, $P_5 = 21.1$ bar.

most PAH products, however, they both produce specific compounds. For benzene pyrolysis, signals from 1-methyleneindene ($C_9H_6CH_2$) and 1-ethynylnaphthalene ($C_{10}H_7C_2H$) were observed. The small peak right before naphthalene might be diethynylbenzene isomers according to the mass spectra. Trace amounts of terphenyl isomers, benzo[*a*]anthracene, benzo[*c*]phenanthrene were detected, which were also observed in phenyl iodide pyrolysis experiments [10]. Peaks of diphenylmethane ($C_6H_5CH_2C_6H_5$) and bibenzyl ($C_6H_5C_2H_4C_6H_5$), with considerable intensities, were only observed in toluene pyrolysis. The quantitative results will be shown later together with the modeling results to illustrate the PAH formation behaviors in benzene and toluene pyrolysis.

3. Kinetic modeling

An aim of this work was to establish a kinetic model to interpret the formation of crucial PAHs from benzene and toluene pyrolysis. First, different literature kinetic models, including the LLNL model [20], JetSurF2.0 [21] and the latest version of CRECK model [22], were tested against the present measurements. Fig. 3 shows that these literature models give distinct predictions for the reactivity of benzene decomposition. This is mainly due to the different phenyl consumption schemes considered in different models. The CRECK model [22] correctly captures the fuel decomposition reactivity and meanwhile well predicts the concentrations of C_2H_2 and C_4H_2 at high temperatures (up to 1700–1800 K) to guarantee a reasonable carbon distribution and balance. It was therefore selected as the basis for the current model development.

Regarding the fuel consumption steps, a modification was made in the decomposition of the linear C_6H_5 (LC_6H_5): two reactions, $LC_6H_5 \rightarrow C_4H_3 + C_2H_2$ and $LC_6H_5 \rightarrow 2C_2H_2 + C_2H$, were included in the original CRECK model [22]. The latter one was removed in the current model due to its redundancy, as the reaction $C_4H_3 \rightarrow C_2H_2 + C_2H$ already existed. This modification does not significantly change the reactivity of the fuels, but slightly improves the predictions for C_2H_2 and C_4H_2 concentrations in comparison to the original CRECK model [22], as shown in **Fig. S3**. Emphasis was put on the formation kinetics of two- to four- ring PAHs in benzene and toluene pyrolysis. Theoretically determined reaction channels and rate constants reported in recent publications were included in the current model. Besides, the current experimental observations were also used to propose possible pathways. All the reactions updated in this work are listed in **Table S1** together with their rate coefficients, and relevant molecular structures are provided in **Fig. S4**. Major points concerning PAH chemistry are described as follows.

C_6H_5 is the most significant product from the initial decomposition steps of benzene, and both the self-recombination and the dissociation of C_6H_5 lead to the formation of o-benzyne (o-C_6H_4) [9,10]. Computed rate coefficients for o-C_6H_4 de-

Please cite this article as: W. Sun, A. Hamadi and S. Abid et al., Probing PAH formation chemical kinetics from benzene and toluene pyrolysis in a single-pulse shock tube, Proceedings of the Combustion Institute, https://doi.org/10.1016/j.proci.2020.06.077

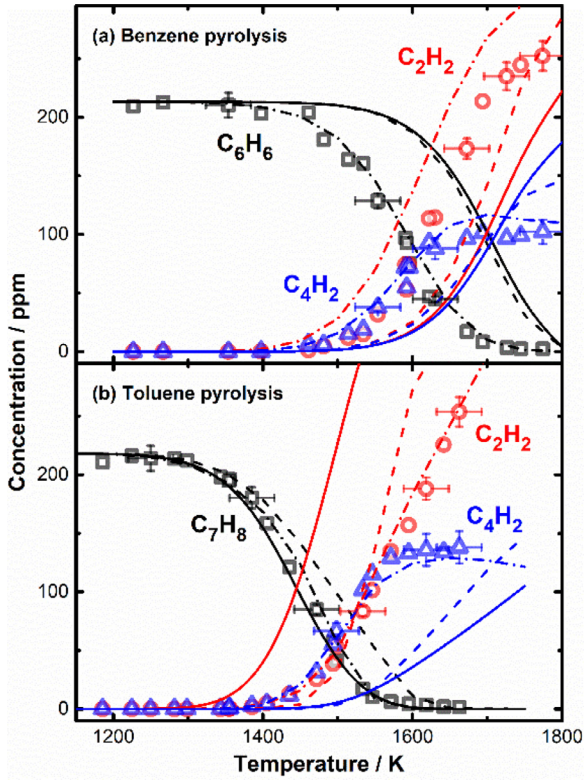

Fig. 3. Predictions by literature kinetic models including the LLNL model (solid lines), JetSurF2.0 (dashed lines) and CRECK model [22] (dash-dotted lines) for fuels, C_2H_2 and C_2H_4 concentrations compared against experimental measurements (symbols) in (a) benzene and (b) toluene pyrolysis.

composition to C_4H_2+C_2H_2 reported by Ghigo et al. [23] were adopted in the current model. Besides fragmentation to smaller species, o-C_6H_4 directly contributes to PAH formation by reacting with aromatic molecules and radicals. The cycloaddition/fragmentation mechanism between o-C_6H_4 and C_6H_6 through the intermediate of benzobicyclo[2,2,2]octatriene (BICYCLO) was proposed by Comandini and Brezinsky [11] to account for the formation of naphthalene ($C_{10}H_8$). o-C_6H_4 self-recombination and the recombination with C_6H_5 leads to biphenylene ($C_6H_4C_6H_4$) and biphenyl radical ($C_{12}H_9$), respectively. Both $C_{12}H_9$ and $C_6H_4C_6H_4$ are involved in the conversion from C_6H_5+C_6H_6 to different $C_{12}H_8$ isomers, as theoretically illustrated by Shukla et al. [12]. Relevant reactions starting from $C_{12}H_9$ were included in a kinetic model to account for acenaphthylene ($AC_{12}H_8$) production in the pyrolysis of phenyl iodide [10]. This reaction sequence was also integrated in the current model. Compared to the pyrolysis of phenyl iodide [10], both H and C_2H_2 are more abundant in the case of benzene pyrolysis, so HACA processes leading to $AC_{12}H_8$ could play a more significant role, as proven by the detection of 1-ethynylnaphthalene ($C_{10}H_7C_2H$) (see Fig. 2(a)). The reactions of $C_{10}H_7$+C_2H_2 producing $C_{10}H_7C_2H$ were included in the model through analogies to the C_6H_5+C_2H_2 → $C_6H_5C_2H$ reaction sequence, for which theoretical pressure-dependent rate coefficients were reported by Mebel et al. [24]. As mentioned above, 1-methyleneindene ($C_9H_6CH_2$) was identified among benzene pyrolysis products. Its radical, benzofulvenyl (C_9H_6CH), was found to be formed in the $C_6H_4C_2H$+C_2H_2 reaction system [24], and this reaction channel has a nonnegligible branching ratio in the investigated temperature range, particularly under high pressure conditions. Given that a cyclopenta-ring already exists in the molecular structure of C_9H_6CH, a HACA route starting from C_9H_6CH is a potential source of acenaphthylene ($AC_{12}H_8$). Such a reaction sequence, as shown in **Fig. S5(a)**, was included in the current model.

It has been well established in previous works [6,14,17] that competing channels respectively leading to benzyl (C_7H_7)+H and C_6H_5+methyl (CH_3) account for the unimolecular decomposition of toluene. The decomposition of C_7H_7 further produces various radicals such as fulvenallenyl (C_7H_5)

Please cite this article as: W. Sun, A. Hamadi and S. Abid et al., Probing PAH formation chemical kinetics from benzene and toluene pyrolysis in a single-pulse shock tube, Proceedings of the Combustion Institute, https://doi.org/10.1016/j.proci.2020.06.077

and propargyl (C_3H_3). Indenyl (C_9H_7) is also supposed to be abundant since indene (C_9H_8) is produced from the reaction between the ubiquitous C_7H_7 and C_2H_2. PAH formation can involve reactions of all the above-mentioned radicals, and such processes were included in the current model. Some of them are explained below. Both C_7H_7+C_3H_3 [16] and C_9H_7+CH_3 [17] reactions lead to the formation of methyleneindanyl radical ($C_9H_7CH_2$) which subsequently converts to naphthalene ($C_{10}H_8$) through dehydrogenation and ring-rearrangement steps [14,16]. A similar reaction scheme was considered to dominate the formation of phenanthrene ($C_{14}H_{10}$) [14,16] during toluene pyrolysis through the intermediate hydromethylenefluorene radical ($C_{13}H_9CH_2$) from both C_7H_7+C_7H_5 and fluorenyl radical ($C_{13}H_9$)+CH_3. The above-mentioned reaction schemes are shown in **Fig. S5(b)** for clear illustration. The C_3H_3 addition to C_9H_7 eventually leads to acenaphthylene ($AC_{12}H_8$), according to a multi-step process proposed recently [25]. The observed diphenylmethane ($C_6H_5CH_2C_6H_5$) peak and the intense signal of fluorene ($C_{13}H_{10}$) (See Fig. 2(b)) can be rationalized by the recombination of C_7H_7 and C_6H_5 leading to $C_6H_5CH_2C_6H_5$ which converts to $C_{13}H_{10}$ through subsequent dehydrogenation. The C_7H_7 self-combination and the recombination of C_7H_7+C_9H_7 were found to respectively result in the formation of $C_{14}H_{10}$ and $C_{16}H_{10}$ isomers in recent theoretical and modeling works by Sinha and coworkers [26,27].

Simulations in this work were performed with the homogenous reactor model of the software COSILAB [28], with a nominal reaction time of 4.0 ms under the constant pressure of 20 bar. The constant pressure simplification for speciation simulations in single-pulse shock tubes was well justified in a recent work [29].

4. Results and discussion

In this section, predictive abilities of the kinetic model will be compared with the speciation measurements. More importantly, the formation pathways of crucial PAH species will be illustrated via the combination of experimental observations and kinetic modeling analysis. We will comparatively discuss the benzene and toluene pyrolysis results, so as to reveal both common and fuel-specific reaction pathways, as well as their temperature dependent behaviors.

4.1. Fuel decomposition and mono-aromatic ring intermediates

Experimental and model-predicted concentrations of fuels and products containing single aromatic ring are illustrated in Fig. 4 as a function of T_5. Modeling results with the CRECK model

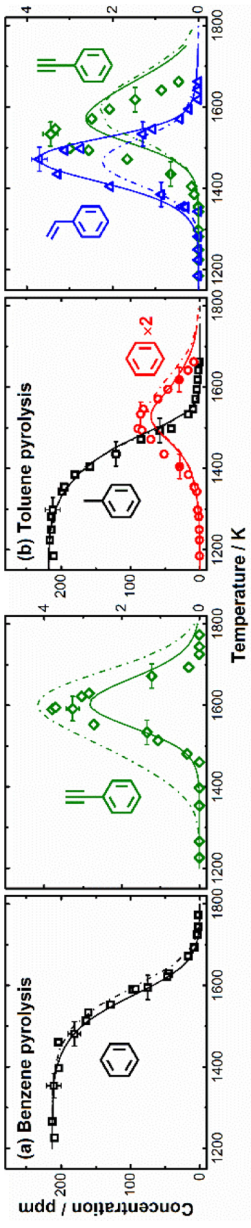

Fig. 4. Concentrations for fuels and mono-ring aromatic products as a function of T_5 in (a) benzene and (b) toluene pyrolysis experiments at the nominal P_5 of 20 bar. Symbols: measurements; Solid lines: simulations with the current model; Dash-dotted lines: simulations with CRECK model [22].

Please cite this article as: W. Sun, A. Hamadi and S. Abid et al., Probing PAH formation chemical kinetics from benzene and toluene pyrolysis in a single-pulse shock tube, Proceedings of the Combustion Institute, https://doi.org/10.1016/j.proci.2020.06.077

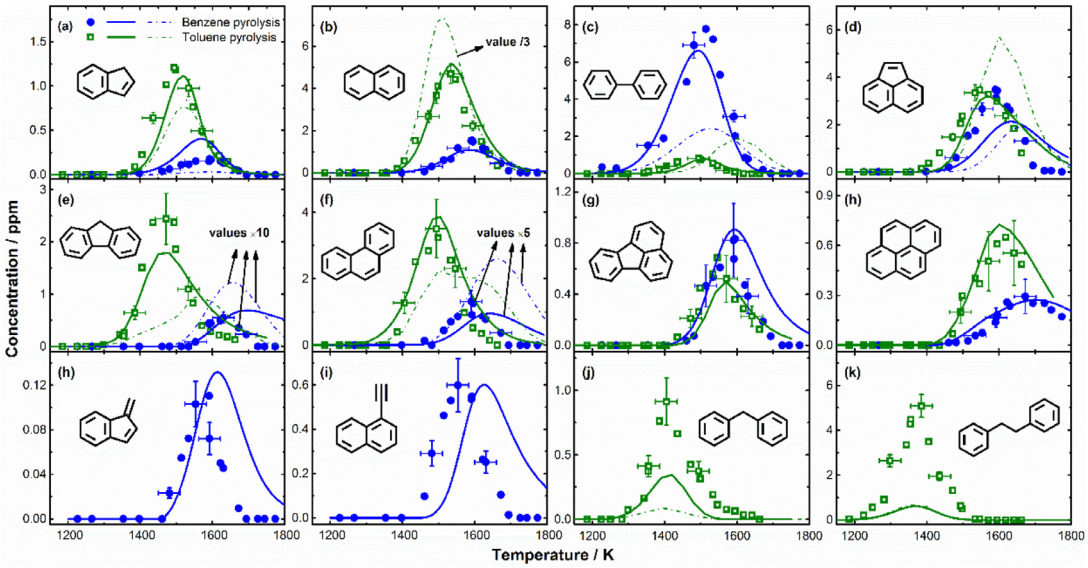

Fig. 5. PAH species concentrations as a function of T_5 in benzene and toluene pyrolysis experiments at the nominal P_5 of 20 bar. Symbols: measurements; Solid lines: simulations with the current model; Dash-dotted lines: simulations with CRECK model [22].

[22] are also shown as a reference. The current model can well capture the fuel reactivity as well as the concentration profiles of the shown intermediates. According to the rate-of production (ROP) analysis, under the current high-pressure pyrolysis conditions, the consumption of benzene is mainly through hydrogen abstraction by H atom over the investigated temperature range. For toluene, unimolecular decompositions and hydrogen abstractions together lead to the fuel consumption, with the latter more dominant at higher temperatures. The chain initiation through hydrogen atom loss from benzene requires relatively high energy. Consequently, the consumption of benzene, compared to toluene, starts at a higher temperature. C_6H_6 produced from toluene pyrolysis is mainly through the reaction $C_7H_8+H=C_6H_6+CH_3$, which contributes almost a constant amount of 10–15% to the fuel consumption at different temperatures. Yuan et al. [17] noted the same branching fraction in flow tube reactor pyrolysis experiments under sub-atmospheric pressure conditions. $C_6H_5C_2H_3$, which originates from the recombination of C_7H_7 and CH_3, was only observed in toluene pyrolysis. $C_6H_5C_2H$ is present in the species pools of both benzene and toluene pyrolysis, but formed in different temperature ranges. The HACA route through $C_6H_5+C_2H_2$ is an important source for $C_6H_5C_2H$ in both cases, but in toluene pyrolysis, the decay of $C_6H_5C_2H_3$ plays a dominant role, resulting in a peak $C_6H_5C_2H$ concentration at a lower temperature.

4.2. PAH species formation

Concentration profiles for PAHs containing two to four rings, including both measurements and simulations, are presented in Fig. 5. The species observed in the pyrolysis of both fuels are shown in the first two rows, while the fuel-specific ones are shown in the third row. The CRECK model [22] gives decent predictions for most shown species because it already incorporate recent theoretically-determined rate coefficients, such as those for benzyl (C_7H_7) decompositions [7,8] and the HACA routes [24]. The current model, however, improved the predictions of both PAH concentrations and formation temperature windows, mainly due to the inclusion of some missing pathways, as will be detailed later in this section. Besides, isomers of $C_{14}H_{10}$ (phenanthrene and anthracene) and $C_{16}H_{10}$ (pyrene and fluoranthene), lumped in the CRECK model [22], were separated in the current model. For PAHs produced from the pyrolysis of both fuels, differences are visible regarding their concentrations and temperature windows. PAH formation pathways, based on the ROP analysis at T_5=1500 K in benzene pyrolysis and T_5= 1400 K in toluene pyrolysis, where most PAH species have considerable concentrations in each case, are displayed in Fig. 6. The shown pathways start from the respective fuel radicals, C_6H_5 and C_7H_7. Both radicals are highly involved in the formation of larger species as an aromatic ring already exists in their molecules, even though the decomposition reactions dominate

Please cite this article as: W. Sun, A. Hamadi and S. Abid et al., Probing PAH formation chemical kinetics from benzene and toluene pyrolysis in a single-pulse shock tube, Proceedings of the Combustion Institute, https://doi.org/10.1016/j.proci.2020.06.077

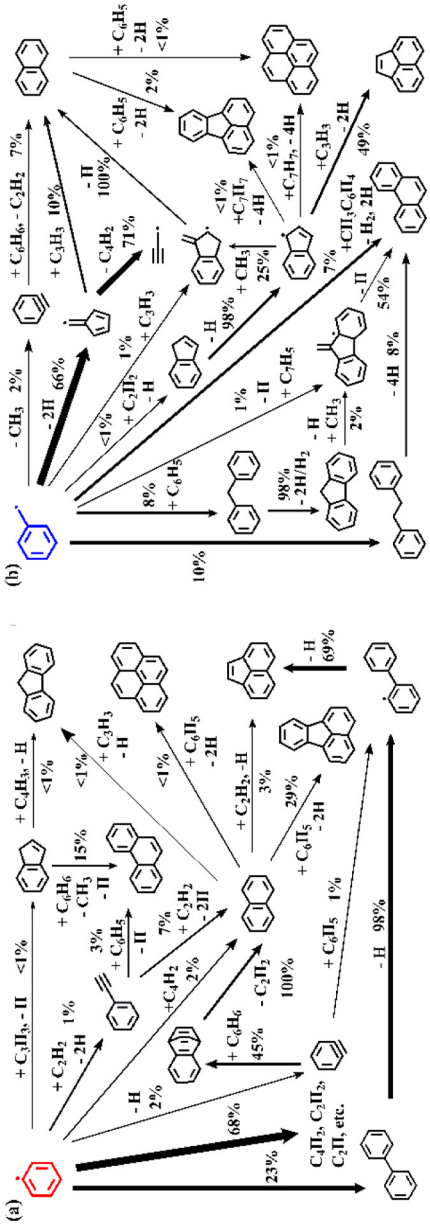

Fig. 6. Major PAH formation pathways starting from fuel radicals in (a) benzene pyrolysis at $T_5 = 1500$ K and (b) toluene pyrolysis at $T_5 = 1400$ K. The thickness of the arrows represents the carbon flux through the corresponding reactions. The numbers represent the percentage contributions of corresponding reactions to the consumption of the species on the source sides of the arrows.

their consumption. C_6H_5 mostly decomposes to small C_4 and C_2 molecules, while C_7H_7 decomposes into smaller radicals such as fulvenallenyl (C_7H_5) and propargyl (C_3H_3), which also have resonantly-stabilized structures. Since C_6H_5 is also abundant in toluene pyrolysis, most pathways in Fig. 6(a) also have certain contributions to the PAH formation in toluene pyrolysis.

Self-recombination reactions of C_6H_5 and C_7H_7 carry considerable carbon flux in the case of benzene and toluene pyrolysis, respectively. The resulting biphenyl ($C_6H_5C_6H_5$) and bibenzyl ($C_6H_5C_2H_4C_6H_5$) are actually the most abundant PAH species measured in corresponding cases. The kinetic model can well predict the concentration distributions of $C_6H_5C_6H_5$, however it underestimates the concentrations of $C_6H_5C_2H_4C_6H_5$ whose formation only requires the participation of the highly stabilized C_7H_7. Considerable amounts of C_7H_7 may still be present when the temperature drops due to the arrival of rarefaction waves and therefore carry on relevant reactions in the quenching period, as pointed out by Mertens et al. [30]. Simulations were performed with measured pressure profiles covering the quenching processes for toluene pyrolysis at 1385 K, 1435 K and 1498 K up to a time scale of 8.0 ms, and the time-dependent species concentration profiles are provided in **Fig. S6** in the ***Supplemental Material***. Relatively high concentrations (from a few to around 20 ppm) of C_7H_7 remain in the reaction system by the end of the heating periods, resulting in the majority of observed $C_6H_5C_2H_4C_6H_5$ produced in during quenching. Differently, the formation of other PAH species is essentially completed before the cooling that occurs at about 4.0 ms. The simulated $C_6H_5C_2H_4C_6H_5$ concentration profile with measured pressure profiles is shown in **Fig. S7** together with the measurement and the simulation within 4.0 ms at constant pressure of 20 bar. The final concentrations of bibenzyl are slightly over-predicted by the current model.

$C_{12}H_9$, the radical of $C_6H_5C_6H_5$, leads to acenaphthylene ($AC_{12}H_8$) through a progressive isomerization process [10,12], and this reaction sequence is the principal source of $AC_{12}H_8$ formation in benzene pyrolysis, according to the modeling analysis. Much less $C_6H_5C_6H_5$, and thus $C_{12}H_9$, is produced from toluene pyrolysis, however, $AC_{12}H_8$ has comparable concentrations with those in benzene pyrolysis, as a consequence of the predominant $AC_{12}H_8$ formation channel through C_3H_3 addition to indenyl (C_9H_7) in toluene pyrolysis. The HACA pathway through naphthyl ($C_{10}H_7$)+C_2H_2 contributes around 5% to $AC_{12}H_8$ formation in both cases, and this value increases to over 30% at higher temperatures (>1600 K). It is noticeable that the current model improves the predictions for $AC_{12}H_8$ concentrations at lower temperatures, owing to the inclusion of above-mentioned fuel-specific reaction schemes. Indene (C_9H_8) has much

Please cite this article as: W. Sun, A. Hamadi and S. Abid et al., Probing PAH formation chemical kinetics from benzene and toluene pyrolysis in a single-pulse shock tube, Proceedings of the Combustion Institute, https://doi.org/10.1016/j.proci.2020.06.077

higher abundance in toluene pyrolysis, as a result of the direct formation from C_2H_2 addition to C_7H_7. The current model can better capture C_9H_8 concentrations in both cases, compared to the CRECK model [22], mainly because C_9H_8 decomposition reactions were updated according to a recent work by Jin et al. [25]. Different reaction patterns lead to naphthalene ($C_{10}H_8$) formation in benzene and toluene pyrolysis: The pathway of o-C_6H_4+C_6H_6 through the intermediate BICYCLO [11] is a dominant source of $C_{10}H_8$ in benzene pyrolysis. In toluene pyrolysis, this reaction also accounts for about 20% $C_{10}H_8$ formation which is governed by the recombination reaction of C_7H_5+C_3H_3 and the ring-rearrangement of methylene-indanyl radical ($C_9H_7CH_2$). $C_9H_7CH_2$ is mainly formed through C_3H_3 addition to C_7H_7 and a minor channel through CH_3+C_9H_7. In both reaction networks, the HACA route through $C_6H_5C_2H$ has limited contribution to $C_{10}H_8$ formation, but it has more pronounced effects at higher temperatures. Fluorene ($C_{13}H_{10}$) has much higher concentrations in toluene pyrolysis, because it directly results from the dehydrogenation of diphenylmethane ($C_6H_5CH_2C_6H_5$) subsequent to C_7H_7+C_6H_5 recombination. While in the case of benzene, $C_{13}H_{10}$ comes from the recombination reactions of C_9H_7+C_4H_3 and naphthyl ($C_{10}H_7$)+C_3H_3. Neither of the channels is efficient due to the insufficient production of C_9H_7 and C_3H_3. Fluorenyl ($C_{13}H_9$) combines with CH_3, aiding the formation of 9-methylenefluorene ($C_{13}H_8CH_2$) which predominantly comes from C_7H_7+C_7H_5 recombination. $C_{13}H_8CH_2$ subsequently converts to phenanthrene ($C_{14}H_{10}$), and this pathway was considered to prevail the $C_{14}H_{10}$ formation in toluene pyrolysis, according to [14]. However, the recombination of C_7H_7 with methylphenyl ($CH_3C_6H_4$) was analyzed to be a greater contributor to $C_{14}H_{10}$ formation with the current model. The fuel-specific reaction schemes explain the abundance of $C_{14}H_{10}$ in toluene pyrolysis. Little amount of $C_{14}H_{10}$ is produced, mainly through the reaction channels of $C_6H_5C_2H$+C_6H_5 and C_9H_7+C_6H_6, in benzene pyrolysis. The isomer pair pyrene ($PC_{16}H_{10}$) and fluoranthene ($FC_{16}H_{10}$) were detected and model-predicted in this work. $FC_{16}H_{10}$ mainly comes from the recombination of naphthyl ($C_{10}H_7$) and C_6H_5 in both benzene and toluene pyrolysis. While in the case of toluene, the dehydrogenation steps starting from C_7H_7+C_9H_7 recombination [27] also yields a small part of $FC_{16}H_{10}$. This reaction channel, processing through a phenylnaphthyl intermediate, can end up with both $FC_{16}H_{10}$ and $PC_{16}H_{10}$. However, it mainly leads to $FC_{16}H_{10}$ at short time scales, as pointed out by Sinha et al. [27]. The recombination of C_6H_5 and $C_{10}H_7$ and a HACA route through phenanthrenyl ($C_{14}H_9$)+C_2H_2 are the dominant sources of $PC_{16}H_{10}$ in benzene and toluene pyrolysis, respectively.

5. Conclusions

A single-pulse shock tube coupled to GC/GC–MS was employed to conduct benzene and toluene pyrolysis experiments at a nominal post-shock pressure of 20 bar over a temperature range of 1100–1800 K. Concentrations as a function of temperature for common as well as fuel-specific PAH products were obtained from respective reaction systems. A kinetic model was proposed based on the latest CRECK model and it showed satisfactory predictive performances for speciation measurements. The improvements in the current model predictive performances lie in the inclusion of some missing but important PAH formation pathways, such as the naphthalene formation through a cycloaddition/fragmentation mechanism between benzene and benzyne, the acenaphthylene formation through ring-closure steps of biphenyl radical and the recombination of indenyl and propargyl. With the combination of experimental measurements and further modeling analysis, formation pathways of two to four ring PAH species during benzene and toluene pyrolysis were illustrated. In benzene pyrolysis, the self-recombination of phenyl results in high concentrations of biphenyl and this non-fused PAH species is found as an important precursor of acenaphthylene, a fused PAH species with the same carbon atom number. Important PAH formation pathways from benzene pyrolysis also have certain contributions in the case of toluene, where pathways initiating from radical recombination reactions, especially those involving resonantly-stabilized radicals, dominate the formation of most PAH species.

Declaration of Competing Interest

The authors declare that they have no known competing financial interests or personal relationships that could have appeared to influence the work reported in this paper.

Acknowledgment

This project has received funding from the European Research Council (ERC) under the European Union's Horizon 2020 research and innovation program (grant agreement No. 756785).

Supplementary materials

Supplementary material associated with this article can be found, in the online version, at doi:10.1016/j.proci.2020.06.077.

References

[1] T. Malewicki, K. Brezinsky, *Proc. Combust. Inst.* 34 (2013) 361–368.

[2] H. Wang, R. Xu, K. Wang, C.T. Bowman, R.K. Hanson, D.F. Davidson, K. Brezinsky, F.N. Egolfopoulos, *Combust. Flame* 193 (2018) 502–519.
[3] A. Laskin, A. Lifshit, *Proc. Combust. Inst.* 26 (1996) 669–675.
[4] R. Sivaramakrishnan, K. Brezinsky, H. Vasudevan, R. Tranter, *Combust. Sci. Technol.* 178 (2006) 285–305.
[5] R. Sivaramakrishnan, R.S. Tranter, K. Brezinsky, *J. Phys. Chem. A* 110 (2006) 9388–9399.
[6] S.J. Klippenstein, L.B. Harding, Y. Georgievskii, *Proc. Combust. Inst.* 31 (2007) 221–229.
[7] M. Derudi, D. Polino, C. Cavallotti, *Phys. Chem. Chem. Phys.* 13 (2011) 21308–21318.
[8] D. Polino, C. Cavallotti, *J. Phys. Chem. A* 115 (2011) 10281–10289.
[9] R.S. Tranter, S.J. Klippenstein, L.B. Harding, B.R. Giri, X. Yang, J.H. Kiefer, *J. Phys. Chem. A* 114 (2010) 8240–8261.
[10] A. Comandini, T. Malewicki, K. Brezinsky, *J. Phys. Chem. A* 116 (2012) 2409–2434.
[11] A. Comandini, K. Brezinsky, *J. Phys. Chem. A* 115 (2011) 5547–5559.
[12] B. Shukla, K. Tsuchiya, M. Koshi, *J. Phys. Chem. A* 115 (2011) 5284–5293.
[13] B. Shukla, A. Susa, A. Miyoshi, M. Koshi, *J. Phys. Chem. A* 111 (2007) 8308–8324.
[14] A. Matsugi, A. Miyoshi, *Proc. Combust. Inst.* 34 (2013) 269–277.
[15] A. Matsugi, A. Miyoshi, *Phys. Chem. Chem. Phys.* 14 (2012) 9722–9728.
[16] A. Matsugi, A. Miyoshi, *Int. J. Chem. Kinet.* 44 (2012) 206–218.
[17] W. Yuan, Y. Li, P. Dagaut, J. Yang, F. Qi, *Combust. Flame* 162 (2015) 3–21.
[18] A. Comandini, T. Malewicki, K. Brezinsky, *Rev. Sci. Instrum.* 83 (2012) 034101.
[19] W. Tang, K. Brezinsky, *Int. J. Chem. Kinet.* 38 (2006) 75–97.
[20] W. Metcalfe, S. Dooley, F. Dryer, *Energ. Fuel* 25 (2011) 4915–4936.
[21] H. Wang, E. Dames, B. Sirjean, D. Sheen, R. Tangko, A. Violi, J. Lai, F. Egolfopoulos, D. Davidson, R. Hanson, *A Hightemperature Chemical Kinetic Model of n-alkane (up to n-dodecane), Cyclohexane, and Methyl-, Ethyl-, n-Propyl and n-Butyl-Cyclohexane Oxidation at High Temperatures*, JetSurF, September 19, 2010 version 2.0 http://web.stanford.edu/group/haiwanglab/JetSurF/JetSurF2.0/index.html .
[22] W. Pejpichestakul, E. Ranzi, M. Pelucchi, A. Frassoldati, A. Cuoci, A. Parente, T. Faravelli, *Proc. Combust. Inst.* 37 (2019) 1013–1021.
[23] G. Ghigo, A. Maranzana, G. Tonachini, *Phys. Chem. Chem. Phys.* 16 (2014) 23944–23951.
[24] A.M. Mebel, Y. Georgievskii, A.W. Jasper, S.J. Klippenstein, *Proc. Combust. Inst.* 36 (2017) 919–926.
[25] H. Jin, L. Xing, J. Hao, J. Yang, Y. Zhang, C. Cao, Y. Pan, A. Farooq, *Combust. Flame* 206 (2019) 1–20.
[26] S. Sinha, A. Raj, *Phys. Chem. Chem. Phys.* 18 (2016) 8120–8131.
[27] S. Sinha, R.K. Rahman, A. Raj, *Phys. Chem. Chem. Phys.* 19 (2017) 19262–19278.
[28] COSILAB, *The Combustion Simulation Laboratory*, Rotexo GmbH & Co., KG, Haan, Germany, 2009 Version 3.3.2.
[29] X. Han, J.M. Mehta, K. Brezinsky, *Combust. Flame* 209 (2019) 1–12.
[30] L.A. Mertens, I.A. Awan, D.A. Sheen, J.A. Manion, *J. Phys. Chem. A* 122 (2018) 9518–9541.

Please cite this article as: W. Sun, A. Hamadi and S. Abid et al., Probing PAH formation chemical kinetics from benzene and toluene pyrolysis in a single-pulse shock tube, Proceedings of the Combustion Institute, https://doi.org/10.1016/j.proci.2020.06.077